WATER RESOURCES RESEARCH, VOL. 27, NO. 5, PAGES 783–796, MAY 1991

46

Convective Accelerations and Boundary Shear Stress Over a Channel Bar

PETER J. WHITING AND WILLIAM E. DIETRICH

Department of Geology and Geophysics, University of California, Berkeley

Alternate bars are important features in alluvial channels as they determine flow and transport patterns. They appear fundamental to selection of meander wavelengths and the geometry of bends. Bend flow has been studied extensively: far less study has been made of flow over alternate bars. Field results from Solfatara Creek, a 5.2-m-wide, 0.2–0.7-m-deep gravel bed channel where flow exits an upstream bend and shoals over a bar in a straight reach, are used to examine patterns of flow and the fluid forces determining the flow field. Large cross-sectional area changes, tied primarily to variation in depth, force large stream-wise accelerations and substantial cross-stream flow off the central bar. The topographically driven downstream and cross-stream accelerations are sufficiently large that their influence upon the balance of forces is of the same order as the pressure gradient and the boundary shear stress. The importance of convective accelerations in the downstream flow equation in this straight reach concurs with bend flow results, but the similar importance of convective accelerations in the cross-stream equation contrasts with results from bend flow. While part of the difference may be attributed to the lower stage conditions herein, in the absence of significant curvature change the cross-stream force balance depends upon the flow going over and around the bar. Local boundary shear stress estimated from the law-of-the-wall and a roughness algorithm decreases out of the upstream bend, increases over the bar top to values approaching the threshold for motion, and then decreases in deeper flow. Strong bed surface coarsening maintains the topography in a stress field that would otherwise lead to planation of the bar top and filling of the deeper regions.

INTRODUCTION

Bars are present in most sand and gravel bed rivers and exert a strong influence on flow and sediment transport processes and, consequently, on channel morphology. In single-thread channels, researchers have generally recognized two bar types: free and forced [*Seminara and Tubino*, 1989]. Migrating free bars develop spontaneously in straight to gently curved mobile channels. Forced bars are thought to develop in response to curvature in channels that, because of their geometry, would not give rise to free bars.

Forced bars are well known from meandering rivers, and their morphology has been studied extensively [*Bluck*, 1971; *Friedkin*, 1945]. Their form includes the shoal on the inside of the bend and the pool along the same bank upstream. As such, the point bar, as it is commonly called, represents only the most shallow part of the form. If the length of forced bars is considered to be the downvalley distance from bar front to bar front along the same side of the channel, most have a wavelength near 10 channel widths [*Leopold and Wolman*, 1960]. Forced bars are nearly steady features that move only as the bend migrates. Field studies [*Bridge and Jarvis*, 1982; *Dietrich and Smith*, 1983, 1984; *Thorne et al.*, 1985] and flume investigations [*Friedkin*, 1945; *Hooke*, 1975; *Odgaard and Bergs*, 1988] have documented flow and transport patterns in bends over such bars, and this research has synergistically validated aspects of bend flow theory [*Engelund*, 1974; *Ikeda et al.*, 1981; *Smith and McLean*, 1984] and motivated further study. As a consequence of the theoretical and experimental work, a fairly advanced developmental view of point bars has emerged. The barform develops from the convergence of sediment from near-bed inward flow in the pool near the concave bank (due to channel curvature [*Dietrich and Smith*, 1983]), and outward flow near the convex bank (due to topographic forcing [*Dietrich and Smith*, 1983; *Nelson and Smith*, 1989]).

Free alternate bars are recognized for their fundamental structure [*Kinoshita*, 1961] that is a consequence of the instability of the coupling between sediment and flow [*Parker*, 1976]. Alternate bars have a characteristic length between bar fronts on the same side of the channel of 6–12 channel widths [*Ikeda*, 1984], and the bars migrate downstream when the bed is mobile [*Kinoshita*, 1961; *Leopold*, 1982]. While it is in the straight channel where free bars are best known, alternate bars in bends, and particularly in the gently curved reaches connecting bends, are common. *Keller and Melhorn*, [1973] and *Hooke and Harvey* [1983] recognized that the distance between scour holes or pools (independent of which side the scour was located) was a fairly consistent 3–7 channel widths in straight and curved reaches. These observations are similar to the earlier recognition by *Kinoshita* [1961] that tortuous meanders of the Ishikari River in Japan contain multiple scour holes that he interpreted as the manifestation of alternate bars. The distinctive morphology of alternating bar fronts skewed across the channel forms as flow diverges off the rising bar top which in turn forces a lateral sediment flux into the adjacent pool.

Recent theoretical work has highlighted the potential importance of interactions between curvature-induced forced bars and free bars in determining the amplitude of the point bar [*Blondeaux and Seminara*, 1985] and suppressing the migration of free bars, thereby establishing the regularity of meander wavelength [*Ikeda et al.*, 1981; *Blondeaux and Seminara*, 1985]. These formerly migration bars are sometimes called fixed bars [*Ikeda*, 1989]. Exploration of these interactions and further progress on the mechanics of flow over the free bars requires basic data on topography and flow sufficiently detailed to test theory. Surprisingly, such data are lacking.

Since the most common location for alternate bars is arguably in the relatively straight reaches connecting bends

Paper number 91WR00083.
0043-1397/91/91WR-00083$05.00

in meandering rivers, this is an appropriate setting for their study. We selected a site on Solfatara Creek in Yellowstone National Park where such bars are common. Our objective was to make a complete set of measurements of flow, sediment transport, water surface, and bed topography at bank-full stage during the spring snowmelt. Unfortunately, the weather did not cooperate, and at best, stage was only one-half bank-full. The most complete data set is for a stage near one-third bank-full, when the bulk of the grain sizes on the bed were immobile. Although with this data we cannot explore empirically the mechanisms controlling the stable morphology and flow fields and their formation, we can examine the influence of bed topography on the flow field and examine how well current theory accounts for the fluid forces involved. These data should provide a crucial test for any detailed mechanistic theory. Because of the low discharge and the bar interaction with the bank, the depth minimum away from the bank typically found on alternate bars nearly forms an island. Hence these data, additionally, may provide some insight to braid bar mechanisms by showing how flow bifurcates around a central hump. These field observations represent an extreme case of topographic control on flow fields.

The primary questions to be addressed here are as follows: What forces arise due to the topographic forcing? Are these included in current theory? Must convective acceleration terms be included in the governing equations? Are there approximations made for the case of point bar theory that are not appropriate for the alternate bar? The issues addressed for the case of flow are similar to those considered in a number of recent papers on flow in meander bends, specifically, the importance of convective accelerations.

EQUATIONS DESCRIBING FLOW

In order to describe steady flow in a channel with varying curvature and topography, *Smith and McLean* [1984] expressed the governing equations in an orthogonal, curvilinear coordinate system following the channel trace. They defined coordinates s parallel to the channel centerline, n perpendicular to the centerline, and z perpendicular to the hypothetically planar bed. The origin of z is at the bed surface. The coordinates are positive downstream, toward the left bank, and upward, respectively. The downstream, cross-stream, and vertical force balance equations and the continuity equation are

$$(\tau_{zs})_b = -\frac{\rho g h}{(1-N)}\frac{\partial E}{\partial s} - \rho\frac{1}{(1-N)}\frac{\partial}{\partial s}\langle u_s^2\rangle h - \rho\frac{\partial}{\partial n}\langle u_s u_n\rangle h + 2\rho\frac{\langle u_s u_n\rangle h}{(1-N)R} \quad (1)$$

$$(\tau_{zn})_b = -\rho g h\frac{\partial E}{\partial n} - \rho\frac{\langle u_s^2\rangle h}{(1-N)R} - \rho\frac{1}{(1-N)}\frac{\partial}{\partial s}\langle u_s u_n\rangle h - \rho\frac{\partial}{\partial n}\langle u_n^2\rangle h + \rho\frac{\langle u_n^2\rangle h}{(1-N)R} \quad (2)$$

$$P_z = \rho g(h - z) \quad (3)$$

$$\frac{1}{1-N}\frac{\partial\langle u_s\rangle h}{\partial s} - \frac{\langle u_n\rangle h}{(1-N)R} + \frac{\partial\langle u_n\rangle h}{\partial n} = 0 \quad (4)$$

where $(\tau_{zs})_b$ and $(\tau_{zn})_b$ are the downstream and cross-stream components of the boundary shear stress, ρ is the fluid density, g is the gravitational acceleration, h is the local flow depth, E is the water surface elevation, u is the flow velocity with the components in the s and n directions denoted by subscripts, and P is the pressure. R is the centerline radius of curvature with its sign given by n, and N is transverse distance from the centerline divided by the radius of curvature. The term $1/[1 - N]$ is a metric coefficient accounting for differential path length with transverse position. The angle brackets signify that the enclosed quantity has been vertically averaged.

Equation (1) presents the downstream balance between the boundary shear stress and the sum of the pressure gradient force, the change in momentum of the downstream flow in the streamwise direction, the change in downstream momentum in the cross-stream direction, and the force associated with the curvature. Equation (2) presents the cross-stream balance between the boundary shear stress and the sum of the cross-stream pressure gradient force, the centrifugal acceleration (second and fifth terms to the right side of the equality) and the change in cross-stream momentum in the downstream and cross-stream directions (third and fourth terms to the right of the equal sign). The vertical velocity is assumed to be small, and hence the vertical force balance reduces to the hydrostatic condition, as presented in (3). Consequently, the formulation does not account for separated flow. The assumption of small vertical velocities will be discussed further later.

FIELD SITE

Solfatara Creek near Norris Junction in Yellowstone National Park, Wyoming, is a sinuous, clear-flowing, gravel bed channel averaging 5.2-m-wide and 0.4-m-deep, with a water surface slope of approximately 0.0010 (Figure 1). Solfatara Creek is a tributary of the Gibbon River (Figure 1) and drains a 62-km^2 area of Pleistocene Lava Creek tuff with extensive surficial glacial deposits [*Richmond and Waldrop*, 1975]. The area is a geothermal region, and several hot springs discharge into the channel upstream of the study reach. Measurements were made 300 m upstream from the confluence with the Gibbon River where Solfatara Creek flows in a 200-m-wide grassy meadow below tree-covered slopes of glacial outwash deposits. In this region the channel banks are generally vertical to overhanging and are locally indented by small failures of the bank. Banks composed of medium to fine sand and silt are capped by a grassy sod with a rooting depth of 0.4 m. In July of 1986, 0.2-m-high grassy levees adjacent to the channel showed a 1–3 mm veneer of freshly deposited sand.

The reach of channel investigated is a 20-m-long, relatively straight section between two bends. Figure 1 is a topographic map of the channel and adjacent meadow made during the study period of April and May 1987. Flow exits the upstream bend with the deepest portion of the channel along the left bank. With diminishing curvature, rapid shoaling develops along the left bank. Associated with the shoaling, the channel widens; variation in cross-sectional area is dominated by depth changes (Figure 2). Shoaling continues near the channel centerline to section 10 where widening lateral scour tapers the central bar. The downstream edge of the bar is very steep, near the angle of repose, and locally,

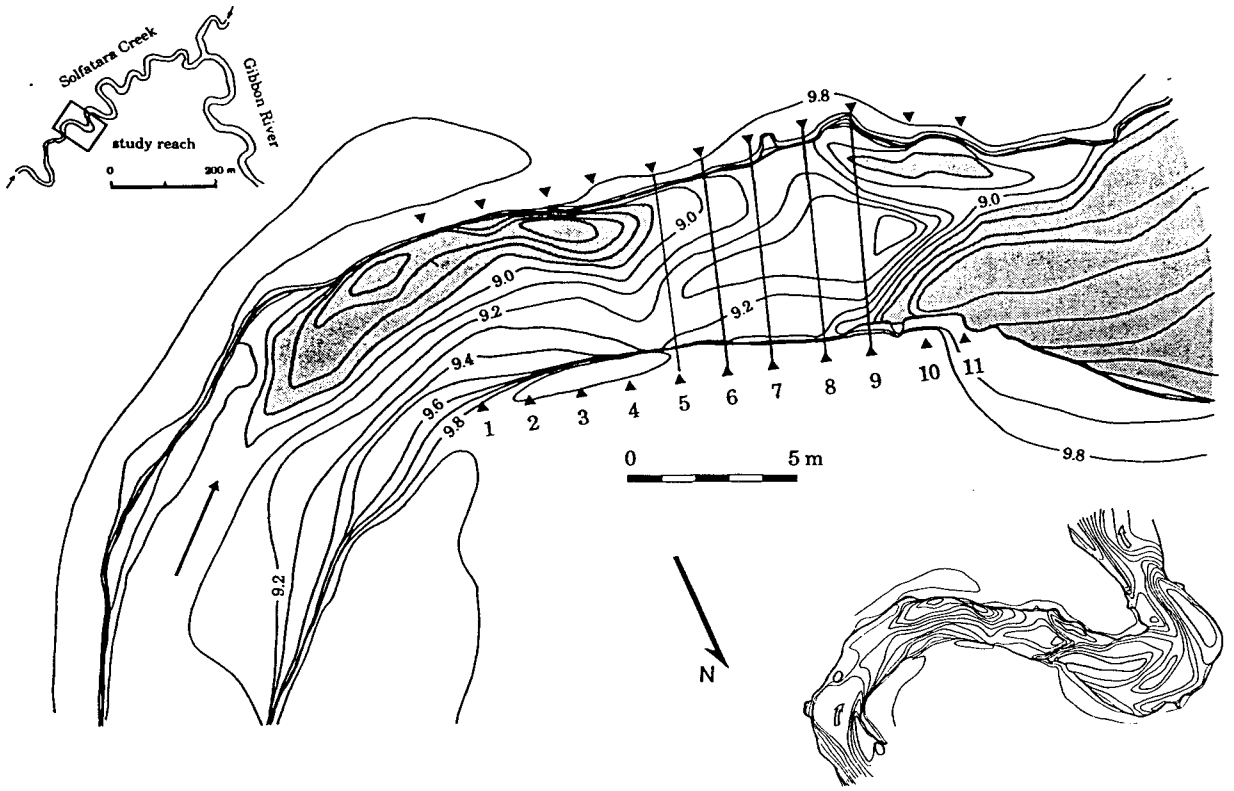

Fig. 1. Topographic map of the field site and location maps. Flow measured at a water surface elevation near section 6 of 9.52 m. Triangles indicate trace of cross sections.

flow separates over the bar front. The marginal channel along the left bank may reflect lower flow dissection of preexisting topography, as inferred from the trend of the 9.0 m and lower contours which do not taper. By this reasoning, at higher stages an oblique bar front spanned the channel with its greatest downstream extent along the left bank. Alternatively, projection of the oblique left bank near section 10 into flow causes the near-bank scour. The unusually broad deep channel from section 10 to the downstream bend may suggest that large barforms are migrating through the sinuous channel. However, comparison of air photos from 1954, 1969, and 1984, show little channel migration in the study reach and no major planform changes upstream and downstream.

Digitization of the centerline at 1-m intervals along the channel defined the curvature of the channel trace. Local bank indentations that nominally widened the section but contained flow fields indirectly related to the main flow field (i.e., separated flows and tranquil areas), were ignored. Except for near upstream sections, the local radius of curvature is very large in the study reach (Figure 3).

The bed surface of Solfatara Creek is composed of fine to medium gravel and coarse sand and is spatially sorted (Figure 4). The median size (D_{50}) of the bimodal bulk distribution is 8 mm, and D_{84} and D_{16} are 16.1 and 0.7 mm, respectively. Subscripts indicate the percentage that is finer. The largest grains are found along the left bank and over the bar top. During the study the gravel was immobile, but loose

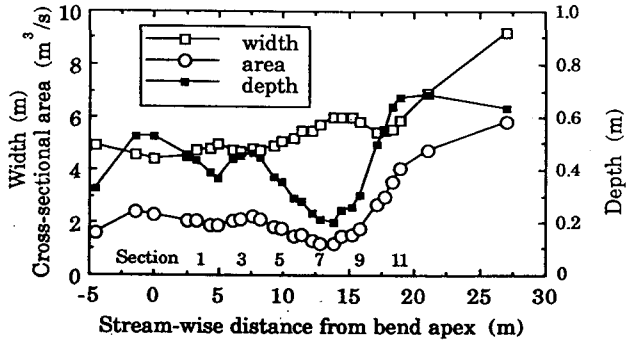

Fig. 2. Cross-sectional area variation (open circles) is largely due to variation in channel depth (solid squares) and not channel width (open squares).

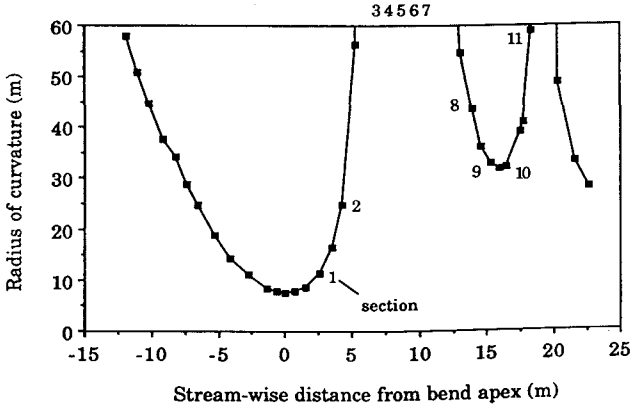

Fig. 3. Absolute value of the radius of curvature along the channel in the vicinity of the study reach. Inset numbers refer to most upstream and downstream sections.

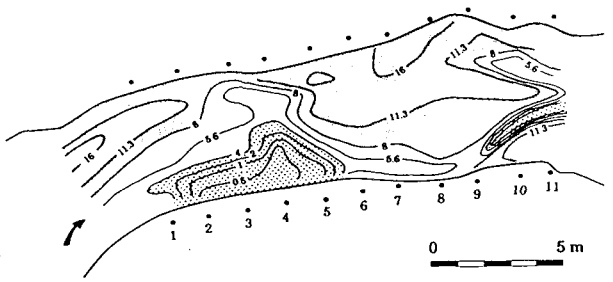

Fig. 4. Map of median grain size in millimeters. The critical boundary shear stress in dynes/cm^2 can be estimated by multiplying the grain size in millimeters by ten.

and easily moved when disturbed, implying recent transport perhaps during the previous season. The subrounded gravel is derived from granite, porphyritic tuff, and obsidian. Sand was locally transported over the gravel bed and deposited in a several centimeter thick layer along the right bank in the lee of the upstream bend and in the lee of the midchannel bar front. In areas without low-flow-deposited sand, the surface was armored; the ratio of the median grain size of the bed surface to that of the subsurface was 1.53. Several pieces of the grassy turf were removed from the bed near the banks at the beginning of the study.

METHODS

Measurements of the flow velocity were made with impeller current meters suspended from a moveable wooden bridge that spanned the channel. The current meters consist of a 3.5-cm-diameter impeller housed in a 1.6-cm-long, 4.2-cm-diameter cage (Figures 5*a* and 5*b*). Small magnets are embedded in two of the four rotor blades. Circuitry in the 1.3-cm-diameter support rod senses a variation in the magnetic field with rotation of the impeller, and a battery-operated counter with a built-in timer records the number of revolutions. Each current meter has an accuracy of ±0.3 cm/s or ±1.2%, whichever is larger [*Smith*, 1978]. Two pairs of meters were mounted 10 cm apart vertically on a vertical metal positioning rod that could be raised and lowered by a handcrank. In each pair the meters were 10 cm apart, orthogonal, and facing upstream such that each meter was oriented 45 degrees to the channel cross section (Figures 5*c*). The upper and lower pairs were 10 and 18 cm upstream of the axis of the 4-cm-diameter positioning rod, and both sets of meters were below the base of the rod (Figure 5*c*). The upper meters were 10 cm below the base of the support rod. The current meters have a cosine response to flow that approaches the meters at angles other than straight-on [*Smith*, 1978], and this calibration for angle of attack is used to iterate for the flow vector whose magnitude and orientation gives the observed readings on each of the orthogonal meters. At 0.2- to 0.4-m intervals across the sections shown on Figure 1, the stacked array of meters was lowered to the bed and the current monitored for a period of 200 s. Successive measurements were made at intervals 2.5 cm higher in the flow for the first 20 cm and then at intervals of 5 cm. In very shallow flow, measurements were made at smaller intervals. In the lee of steep bar fronts and near banks, narrow strips of flexible plastic were used to confirm flow directions determined from the meters. The meters were repeatedly observed through the clear flow to prevent fouling of the meters by organic material or bed material. Only about 2% of the approximately 1700 velocity pairs reported in this paper had to be discarded because of contamination. An average of about 160 paired readings defined the velocity field at each section.

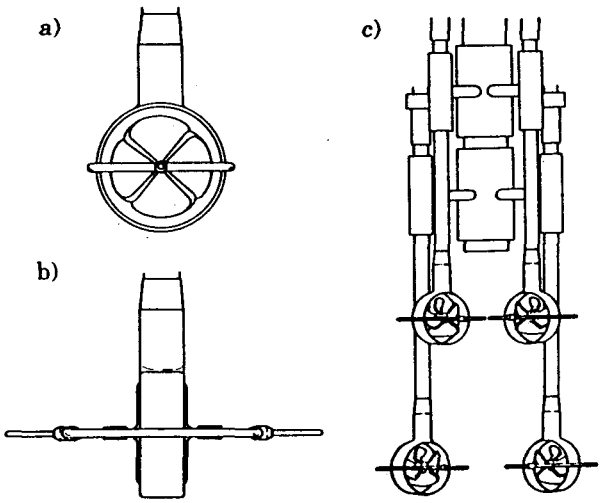

Fig. 5. Current meter and setup (*a*) front view of single meter (*b*) side view of meter (*c*) array of meters on vertical positioning rod. The relative positions of meters, especially with respect to the support rod, have been altered to conserve space.

Water surface topography was measured at 0.2-m intervals across each numbered section, at transects between numbered sections, and at additional transects upstream and downstream of the reach with numbered sections. With one person at the surveying level, the other person, working from the bridge, positioned a stadia rod such that a small pointer attached to the base of the rod just touched the water surface. The rod was repeatedly raised and lowered to the water surface until a consistent reading to within 1 mm was made; this typically took 3–5 tries. On the two occasions water surface topography was measured, stage varied during the 4–5 hours of measurement by 1 and 6 mm. Frequent observations of the water level at a stage plate were used to adjust water surface measurements to a common stage. The results reported herein are for the case when stage varied by 1 mm. A recorder documented major stage changes that occurred during periods when the site was unoccupied. Water temperature typically varied between 8° and 14°C during the day.

The topographic map of the channel and surrounding meadow was made with a level and tape measure. In the channel the water surface served as a datum, and measurements of the distance from the bed to the water surface were recorded and converted to elevation. Depth was measured at 0.2-m intervals across the channel, except closer near the banks, and at about 0.7-m intervals down the channel.

The bed material size was determined at 0.4- to 0.6-m intervals across the sections by scraping 200–300 gm samples from the bed with a miniature sediment sampler. The sampler is similar in design to the Helley-Smith sediment sampler [*Helley and Smith*, 1971] but has a smaller 4-cm-square orifice. Subsurface samples were obtained by a second scraping after the surface had been broken. Sampling of the bed took place after completion of all flow measurement.

Sediment samples were dried in the laboratory and sieved at half-phi intervals.

SECTION ORIENTATION

The selection of the cross-section orientation is critical to the determination of the force balance in a reach of channel because it explicitly defines the cross-stream and downstream components of flow. The approach used herein is presented in greater detail by *Dietrich and Smith* [1983]. In brief, sections are preliminarily selected by eye in the field to be perpendicular to the banks. Measurements are made at these preliminarily oriented sections and the continuity equation used to calculate the local cross-stream flux from differences in the downstream velocity field between sections upstream and downstream of the section under consideration. The calculated local cross-stream fluxes are integrated across the channel to compute the cross-stream discharge for the section from continuity $Q_{nw,c}$, where

$$Q_{nw,c} = \int_{-w/2}^{w/2} \left(\frac{-1}{1-N} \int_{-w/2}^{n} \frac{\partial \langle u_s \rangle h}{\partial s} \, dn \right) dn \qquad (5)$$

The cross-stream discharge for the section from measured local $\langle u_n \rangle$ values, $Q_{nw,m}$, is

$$Q_{nw,m} = \int_{-w/2}^{w/2} \langle u_n \rangle h \, dn \qquad (6)$$

The average direction of flow θ_w between sections with the downstream discharge Q_{sw} is

$$\theta_w = \tan^{-1} \left(\frac{Q_{nw}}{Q_{sw}} \right) \qquad (7)$$

On the basis of the angles computed by inserting the continuity-derived cross-stream flux (5) and the width-integrated measured cross-stream flux (6) into (7), the section orientation is altered to match the flow direction calculated from continuity.

Section alignment as presented in (5), (6), and (7) involves vertically averaged values of downstream and cross-stream velocity. At each position across the channel where velocity profiles were measured, the flow velocities nearest the bed and the water surface were assumed to be invariant to the boundary. Typically, measurements were made 2.2 cm above the bed and within 5 cm of the water surface. Given the weak shear near the surface this assumption of invariance is reasonable. Vertical integration of the measured velocities, from the bed to the water surface, and division by the local depth, yields the vertically averaged velocity.

Section orientation based on cross-stream integration of differences in the downstream discharge is affected by variation in total discharge between sections. These variations arise from nonuniformity of stage and from the methodology of integrating discharge across the channel. The apparent variations in discharge stemming from the integration are partly due to the assumptions used to extrapolate velocities to the bed and water surface and probably largely due to extrapolation of near-bank velocities to the bank.

Stage varied by about 0.4 cm and never by more than 1.0 cm during the 8- to 10-hour period typically required to measure flow across a single section. Day-to-day stage variation was larger and due to precipitation and diminishing snowmelt. A rating curve for the channel was constructed and is shown in Figure 6. Bankfull discharge estimated from extrapolation of the rating curve and from the Manning equation assuming constant slope and roughness is approximately 2.4 m^3/s. Most of the sections were measured at two different stages, and as a result, it is possible to define two data sets with minor stage variation. These stages are 0.52 m and 0.59 m: total discharges of 0.73 and 1.08 m^3/s, respectively. These correspond to fractions of estimated bankfull discharge of 30 and 45%.

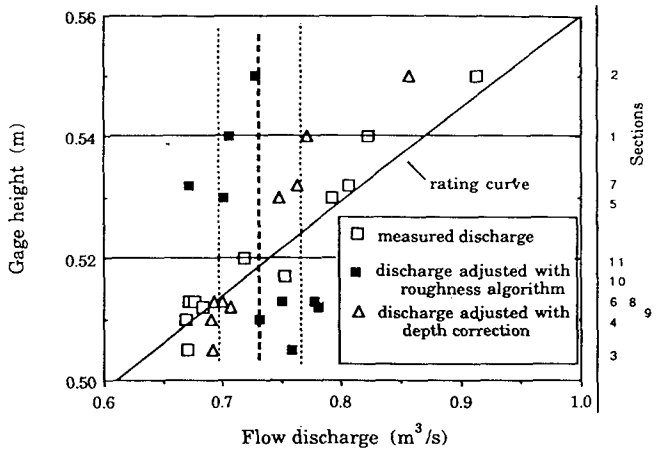

Fig. 6. Rating curve (solid line) and collapse to common stage of 9.52 m for cross-sectional measurements. The open squares represent the measured discharge; the triangles, the adjusted discharge by depth adjustment; and the solid squares, the adjusted discharge by roughness. The dotted vertical lines are the bounds for 4% error about the expected discharge of 0.73 m^3/s. The numbers at the right refer to the section.

The results discussed in this paper are for the stage of 0.52 m and were collapsed to the common stage by several methods (Figure 6). If the difference between the measured stage and the common stage was small, less than 0.01 m, it proved sufficient to adjust the depth, as indicated in Figure 6 by the proximity of the adjusted discharge to the expected discharge of 0.73 m^3/s at a stage of 0.52 m. If the stage difference was larger than 0.01 m, a roughness argument was used to adjust the discharge. The discharge variation about the common stage (0.52 m) was less than 4% at each section and averaged 2%. These small differences were then accounted for by normalization of vertically averaged velocities by the ratio of expected total discharge to recalculated measured discharge. This procedure subsumes discharge variation associated with uncertainty in velocity extrapolation to boundaries.

The normalized vertically averaged velocities were located in the section with respect to the channel centerline as digitized from the planform map. At 25-cm intervals from the centerline, values of the vertically averaged current velocity were calculated by linear interpolation. These values were then used with the continuity equations (4) and (5) to determine the realignment required by continuity. The realignment required of each section averaged 3.0 degrees, with no systematic bias to the initial visual orientations (Table 1). Further recalculation and reorientation was unnecessary.

TABLE 1. Orientation Corrections

Section	Degrees
1	3.3
2	2.1
3	0.2
4	−3.4
5	1.9
6	2.0
7	−0.4
8	−2.5
9	−3.9
10	−0.6

BED AND WATER SURFACE TOPOGRAPHY AND FLOW FIELDS

The bed topography of the study reach is dominated by effects of the upstream bend and the downstream bar. At section 1, near the apex of the bend, the depth is greatest near the outside bank (Figure 1). Downstream to section 4 there is further deepening along the outside (left) bank, while along the right bank the lateral point bar slope is fairly constant through this reach. Below section 4, depth decreases rapidly along the left bank and increases slowly along the right bank. By section 5 the cross section is slightly humped over a developing central bar, and this broad convexity continues to grow downstream to section 8, and the channel widens. Downstream of section 9, deepening on the margins of the central convexity tapers the central bar front. Near the centerline, shoaling continues to near section 10, and at the stages studied the bar top was nearly at the water surface. Downstream of 11 the channel cross section is broad and deep.

Downstream and cross-stream flow fields for the sections at the stage of 0.52 m are presented in Figure 7. The downstream flow field reflects the effect of the upstream bend, the downstream shoaling, and the sudden channel area increase. The high-velocity core is slightly to the left of the center of the channel at the bend apex (near section 1) and drifts further toward the left bank by section 4. The high-velocity core shifts toward the center at 5, then further to the right bank by 6, before bifurcating into two strands of high velocity on either side of the bar. Between sections 8 and 11 these strands are very near the banks. Flow decelerates out of the bend as the section deepens at 3 and 4 and then begins to accelerate to section 8. Maximum downstream velocities are reached at sections 8 and 9 near the banks at the margins of the central hump. The largest acceleration occurs between sections 5 and 6. As flow becomes very shallow near the channel centerline near 9 and 10, the flow decelerates. The low velocities near the margins of the central bar at 10 and 11 are due to flow separation that occurs in the lee of the steep bar front. Past the bar crest, flow decelerates in the larger cross-sectional area.

Without free-surface shear in uniform flow it is normal to observe the maximum downstream flow velocity at the free surface. An interesting characteristic of the Solfatara flow field is the depression of the highest velocities below the water surface, often to very near the bed. This pattern is commonly seen near the banks and where the depth is rapidly diminishing, for example, at section 2, 0.75 m to the left of the centerline, and at much of sections 7 and 8. Figure 8 presents the relative height of maximum velocity scaled by flow depth, compared to the depth gradient downstream. Near-bank measurements have not been included. The highest velocities are below the water surface when depth is decreasing, presumably because rapid shoaling forces substantial near-bed accelerations that cannot be accounted for by lateral flow. The nonmonotonic increase in velocity with distance from the bed questions the assumption of constant vertical velocity structure and suggests the nonvalidity of estimates of shear stress from velocity profiles, a point that will be discussed later.

The cross-stream velocity fields near the apex of the upstream bend show inward flow (toward the right bank) near the bed and outward flow near the surface (Figure 7). With diminishing curvature at section 2, the magnitude of the outward flow (toward the left bank) decreases, and by section 3 the cross-stream flow across most of the section is toward the right bank. At 4, flow is toward the right bank across the whole of the section. Further downstream, flow toward the left bank is confined to regions near the left bank. Over the top of the bar, transverse components of velocity are oriented toward the right bank and are locally greater than one-half the downstream component. At the margins of the bar, surface flow spills laterally off the central hump. In the lee of the bar front, flow directions reflect the orientation of the oblique step. Consequently, two opposing cells of secondary circulation develop on either side of the bar.

The cross-stream flow field is forced by the depth change and less so by the variation in width, as indicated by change in cross-sectional area (Figure 2). An estimate of the lateral flux in the half-space on either side of the centerline can be derived geometrically:

$$\langle \bar{u}_n \rangle = \langle \bar{u}_s \rangle \frac{\Delta w/2}{\Delta s} \tag{8}$$

The overbar indicates that the quantity has been cross-sectionally averaged. Width between sections 1 and 9 increases from 4.6 to 6.0 m over a stream-wise distance of 12.6 m. A reasonable estimate of the average downstream velocity is 40 cm/s. The calculated lateral flux from (8) is 2.2 cm/s, a value that is much smaller than the observed transverse velocity. From section 5 to 9 the lateral flux similarly ascribed to widening from 4.8 to 6.0 m over a distance of 6.5 m is 3.6 cm/s, a value substantially less than the observed lateral velocities reaching 30 cm/s. Width variations which are not explicitly treated in the formulation of the governing equations do not dominate the momentum fluxes in this channel.

The vertically averaged values of downstream and cross-stream velocity used for computation of stresses are shown in Figure 9. Both the general acceleration in $\langle u_s \rangle$ downstream to the bar top and then deceleration past the bar are illustrated well. The cross-stream flux toward the right bank (negative values of $\langle u_n \rangle$) with initial shoaling and divergence in flow directions as flow spills off the bar top are also apparent.

The water surface topography at a stage of 0.506 m is presented in Figure 10. In the upstream bend and downstream to section 4 there is a positive cross-stream tilt to the transverse water surface with a weak, and locally adverse, longitudinal slope. Downstream of section 4, to section 7, the longitudinal water surface steepens, particularly along the right bank, leading to a very steep transverse slope that should act to drive flow toward the right bank. At section 7

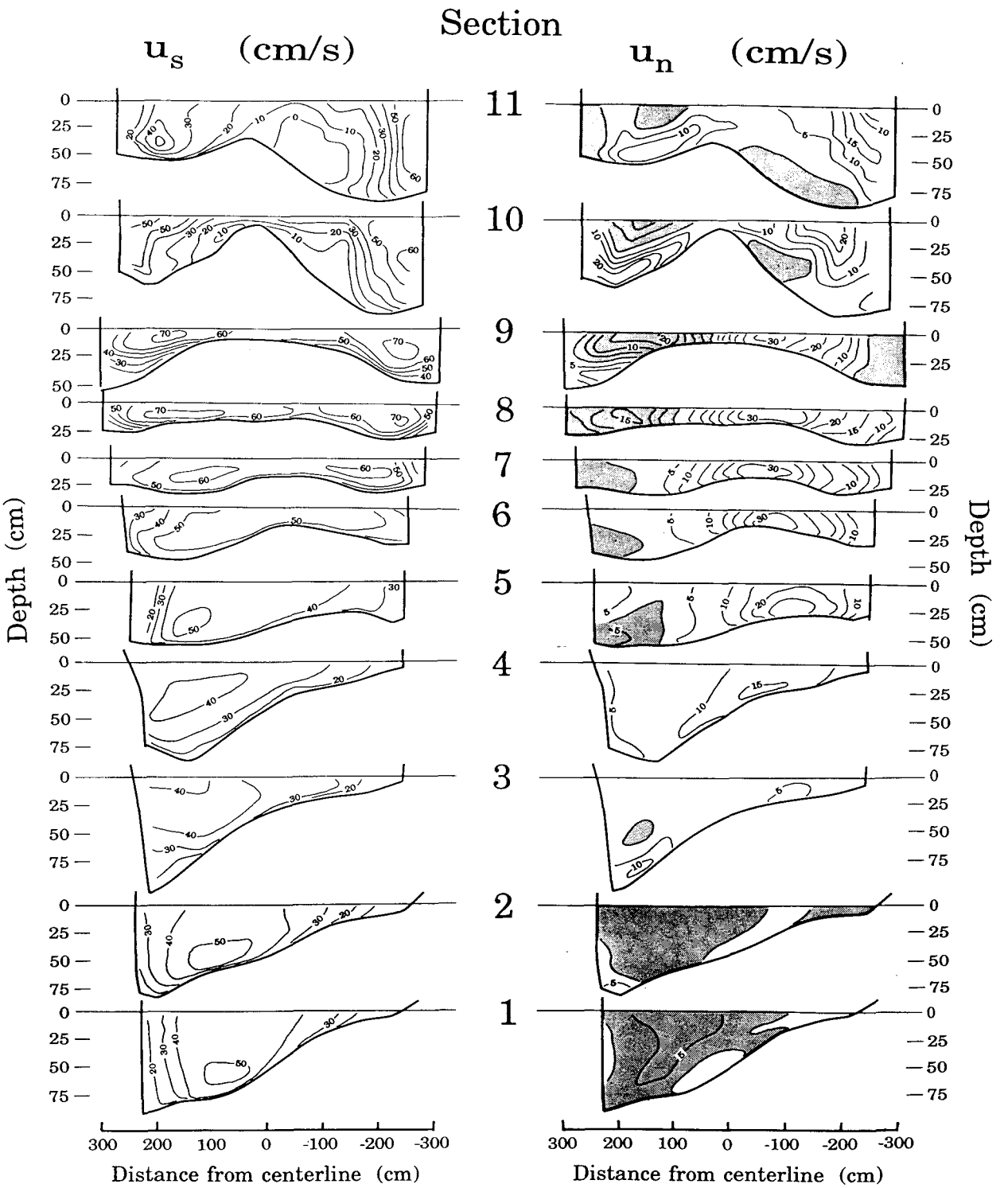

Fig. 7. Downstream and cross-stream velocity fields at sections. These values have been reoriented to conform with continuity and normalized to the common stage. Shaded areas in the cross-stream panel indicate positive values (flow toward the left bank).

the longitudinal water surface along the left bank drastically steepens, gradually reducing the transverse slope. Transverse slopes at 7 and 8 force flow off the central bar toward the banks. Between sections 8 and 9 the acceleration of flow over the shallow bar top sufficiently depresses the water surface such that downstream, with the rapid increase in depth, there is a pronounced adverse downstream water surface slope. Water surface elevations are rather flat to the downstream bend.

Components of the Force Balance

In the introduction we posed several questions regarding the importance of convective accelerations in the governing

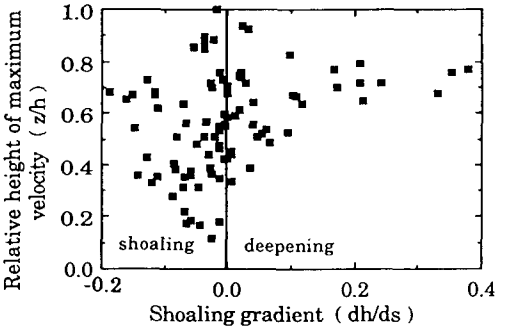

Fig. 8. The maximum flow velocity is relatively closer to the bed with shoaling. The height of maximum velocity is scaled by local flow depth.

equations when curvature was minor that can now be addressed. The approach taken herein is, first, to use a comparison of the predicted and measured water surface slope as an indicator of the precision of measurement and methodology; second, to examine the magnitude of the components that sum to produce the total water surface slope; and third, to present the components of the force balance in the physically meaningful framework of boundary shear stress.

The vertically averaged equations are rewritten, by substitution of the continuity expression (4), into the streamwise and transverse force balance equations (1) and (2) to solve for the downstream and cross-stream water surface slopes. The approximations have been made that $\langle u_s^2 \rangle = \langle u_s \rangle \langle u_s \rangle$, $\langle u_n^2 \rangle = \langle u_n \rangle \langle u_n \rangle$, and $\langle u_s u_n \rangle = \langle u_s \rangle \langle u_n \rangle$ [*Dietrich and Smith*, 1983].

$$S = \frac{(\tau_{zs})_b}{\rho g h} + \frac{\langle u_s \rangle}{g(1-N)} \frac{\partial \langle u_s \rangle}{\partial s} + \frac{\langle u_n \rangle}{g} \frac{\partial \langle u_s \rangle}{\partial n} - \frac{\langle u_s \rangle \langle u_n \rangle}{gR(1-N)} \tag{9}$$

$$S_n = -\frac{(\tau_{zn})_b}{\rho g h} - \frac{\langle u_s \rangle^2}{Rg(1-N)} - \frac{\langle u_s \rangle}{(1-N)g} \frac{\partial \langle u_n \rangle}{\partial s} - \frac{\langle u_n \rangle}{g} \frac{\partial \langle u_n \rangle}{\partial n} \tag{10}$$

For simplicity in the ensuing discussion, (9) and (10) are rewritten to assign each term a label, and so that $S = [-1/1 - N]dE/ds$ and $S_n = dE/dn$:

$$S = S_1 + S_2 + S_{3a} + S_{3b} \tag{11}$$

$$S_n = S_{n1} + S_{n2} + S_{n3} + S_{n4} \tag{12}$$

The total boundary shear stress in the downstream and cross-stream directions was estimated from a drag formulation and rewritten with

$$S_1 = \frac{C_d}{2g} \cos \beta [\langle u_s \rangle^2 + \langle u_n \rangle^2] \tag{13}$$

$$S_{n1} = \frac{C_d}{2g} \sin \beta [\langle u_s \rangle^2 + \langle u_n \rangle^2] \tag{14}$$

β is the near-bed flow direction. The drag coefficient (C_d), calculated by the assumption of uniform downstream flow over many channel widths, has a value of 0.0462. The formulation of S_{n1} explicitly defines the stress direction to be parallel to the near-bed flow direction and hence incorporates the effect of secondary flow.

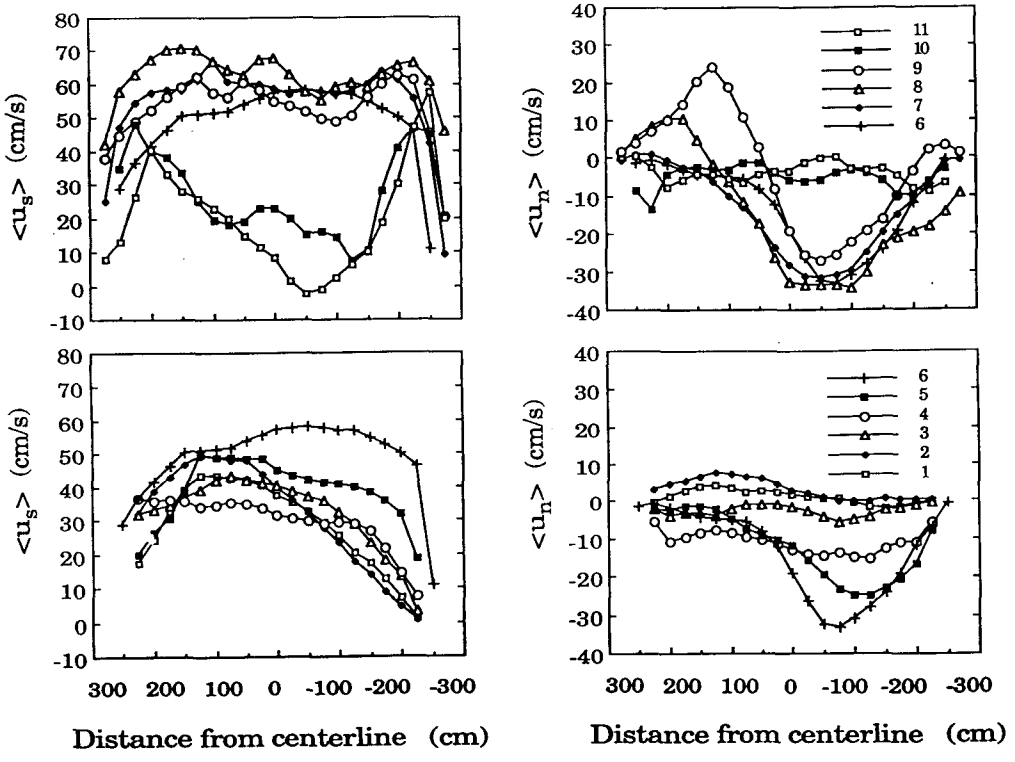

Fig. 9. Interpolated vertically averaged downstream $\langle u_s \rangle$ and cross-stream $\langle u_n \rangle$ velocity values used in calculations.

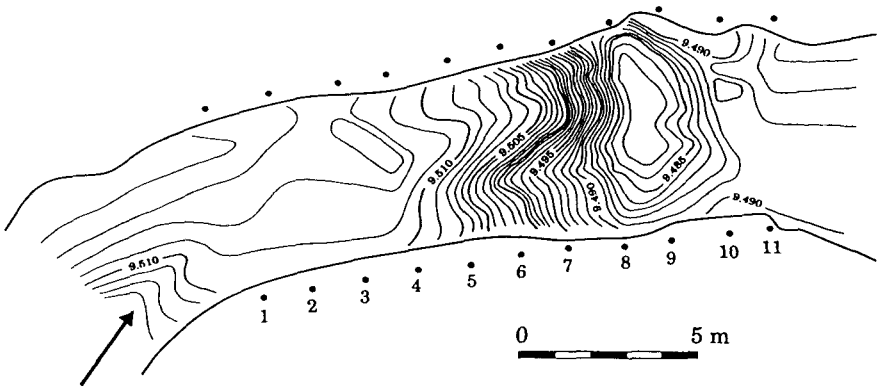

Fig. 10. Water surface elevation at a stage of 9.506 m.

Figure 11 compares the predicted and observed downstream water surface slopes at each section. The observed downstream slopes at sections were computed from the map of water surface elevations over distances of 1.0 m (Figure 10). The calculations (11) correctly predict the observed rather flat downstream water surface slope in upstream sections and the dramatic steepening over the bar. The adverse slopes with deepening past section 9 and the negligible slopes further downstream are predicted as well. The relatively poor reproduction of the magnitude and structure at section 1 stems from its position as the upstream-most section and the consequent poor definition of local downstream velocity divergence. Local slope variation across sections is reproduced well, especially at sections 2–5 and 10. Slightly improved slope prediction could be produced by spatially varying the drag coefficient, that is, to account for different bed sizes, but such a modification violates the premise of uniformity and was not performed.

The success at reproducing the observed slopes depends upon the incorporation of all terms of importance in the governing equations. Figure 12 plots the components of the downstream slope at each section. Components S_1 and S_2, the shear stress term and downstream acceleration term, are important throughout the reach. S_{3a}, representing the cross-stream transport of downstream momentum, while smaller than S_1 and S_2, is important and locally dominates the structure of the slope. Except upstream, S_{3b} is small because of the overall straight nature of the channel. S_{3a} and S_{3b}, while generally of opposite sign in the curved portion of the channel, do not sum to zero. The Solfatara results, while for a different planform and stage, echo the conclusions of *Yen and Yen* [1971] and *Dietrich and Smith* [1983]; the downstream force balance equation must include convective accelerations associated with the cross-stream transport of stream-wise momentum.

The predicted and observed cross-stream water surface slopes are compared in Figure 13. The observed local slope was calculated from the water surface elevation difference over a transverse distance of 0.5 m (Figure 10). The calculations reproduce the observed weak transverse slope associated with the upstream bend and the strong cross-stream slope associated with the shoaling between sections 5 and 9. From sections 5 to 8 the resolution of the finer details of the observed cross-stream slope is noteworthy. Generally, the cross-stream predictions are superior to the downstream, probably because of the closer cross-stream spacing of water surface measurements. While there are some discrepancies between observed and predicted slopes at sections 9 and 10, they are not surprising considering the local flow separation in these areas. The components summing to produce the predicted cross-stream slope are shown in Figure 14. All terms in the cross-stream slope equation (10) are locally important to the balance. S_{n3} and S_{n4}, which account for the effects the downstream and cross-stream transport of cross-stream momentum have on the transverse slope, are generally the largest terms, with the former larger than the latter. From sections 1–4 the transverse slope is dominated by S_{n3}, but with shoaling downstream, S_{n4} becomes significant. The two terms are additive with initial shoaling, which leads to a

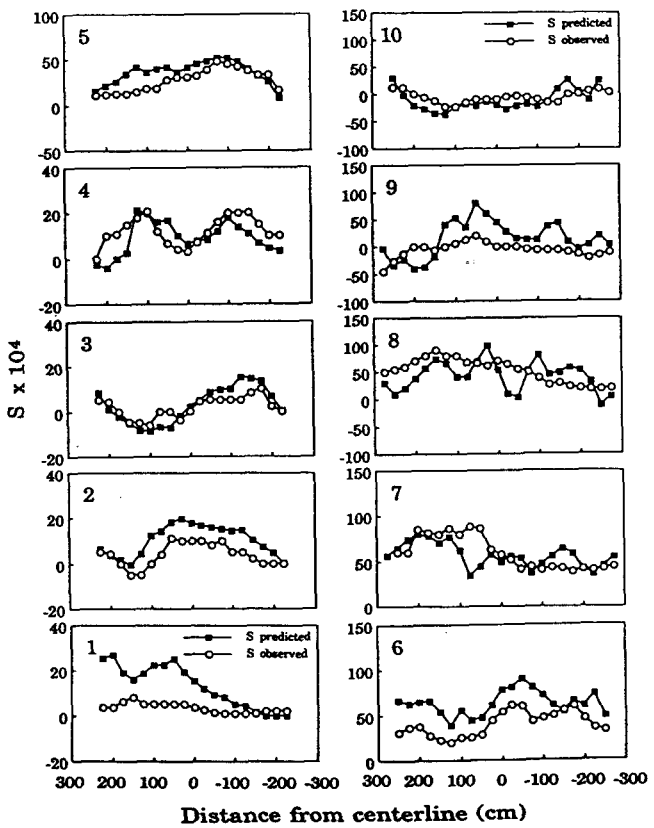

Fig. 11. Predicted and observed downstream water surface slope. Note ordinate scale change between sections 4 and 5 and sections 7 and 8.

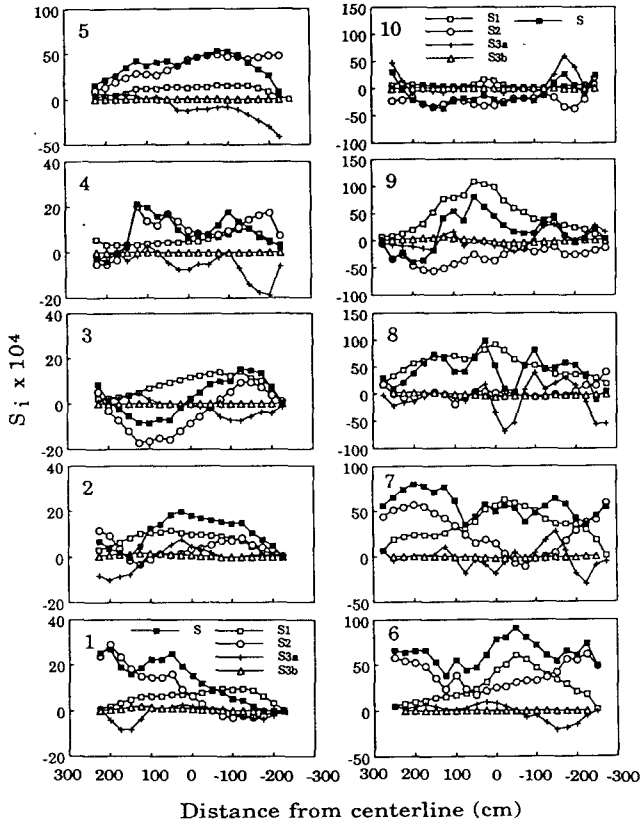

Fig. 12. Components of the downstream slope. Note ordinate scale change between sections 4 and 5 and 7 and 8.

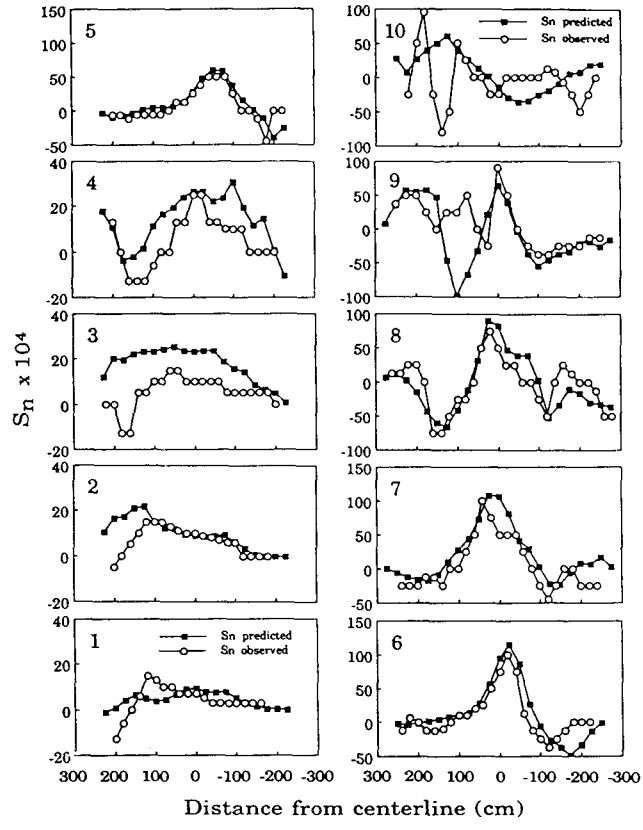

Fig. 13. Predicted and observed cross-stream water surface slopes. Note ordinate scale change between sections 4 and 5.

very steep tilt of the water surface toward the right bank. As the bar top is approached, the decreased topographically induced transverse flow causes the terms to become opposite in sign, reducing the transverse tilt. The centrifugal term S_{n2} is important only at upstream sections where curvature is significant. The effect of the transverse component of the bed shear stress on the transverse slope S_{n1} is large from sections 6 to 9, where it determines the structure of the slope pattern to a significant degree.

Most bend studies have found that the centrifugal term S_{n2} is the dominant term determining the transverse slope. *Dietrich and Smith* [1983], *Dietrich and Whiting* [1989], and *Odgaard and Bergs* [1988] found that the centrifugal term dominated the cross-stream balance and that S_{n3} and S_{n1} were of minor importance. *Odgaard* [1986] pointed to the second-order importance of S_{n3} in giving rise to the overshoot phenomena. *Yen and Yen* [1971] showed that at the crossing of the high velocity core to the outer bank, S_{n3} was as important as the centrifugal term but elsewhere was small. The significance of the Solfatara result is that, in the absence of significant curvature, terms other than the centrifugal force (S_{n2}), determine the slope.

Local Boundary Shear Stress Prediction

Ultimately, the geomorphologist would like to predict the boundary shear stress field in a channel, for it determines the morphologic adjustment of a mobile bed. Calculated boundary shear stress is a difficult parameter to verify because methods to calculate it are based upon assumptions that often do not hold and clearly are inappropriate for the nonuniform flow over the bar. The approach taken herein is to calculate the local boundary shear stress, to compare these results with the stress determined from the governing equations (1) and (2), and to relate the variation in stress and components of the stress to the geomorphology of the channel reach. A similar approach, with a less complete data set, was used to analyze boundary shear stress through a bend [*Dietrich and Whiting*, 1989]. These authors also give a general discussion of various tactics for estimating local boundary shear stress in the field.

A common technique for estimating the local boundary shear stress is to use near-bed velocity profiles and the law-of-the-wall:

$$\tau_b = \rho \left[\frac{ku}{\ln\left(\frac{z}{z_0}\right)} \right]^2 \qquad (15)$$

Three to seven velocity measurements were used to compute shear stress values from (15); all were within 0.2 times the flow depth of the bed. The estimated values of local boundary shear stress from velocity profiles (open circles) seem far too low (Figure 15) in many portions of the channel, given the observation of sand transport and rippled sand along the bar margins and the sensitivity of the surface to disturbance. Furthermore, roughness scales (z_0) from projection of the velocity profile to zero velocity are also far too small ($z_0/k_s \sim 0.01$–0.001) for this alluvial surface. As noted earlier, the velocity profiles show very little shear above a few centimeters in elevation. We conclude that the

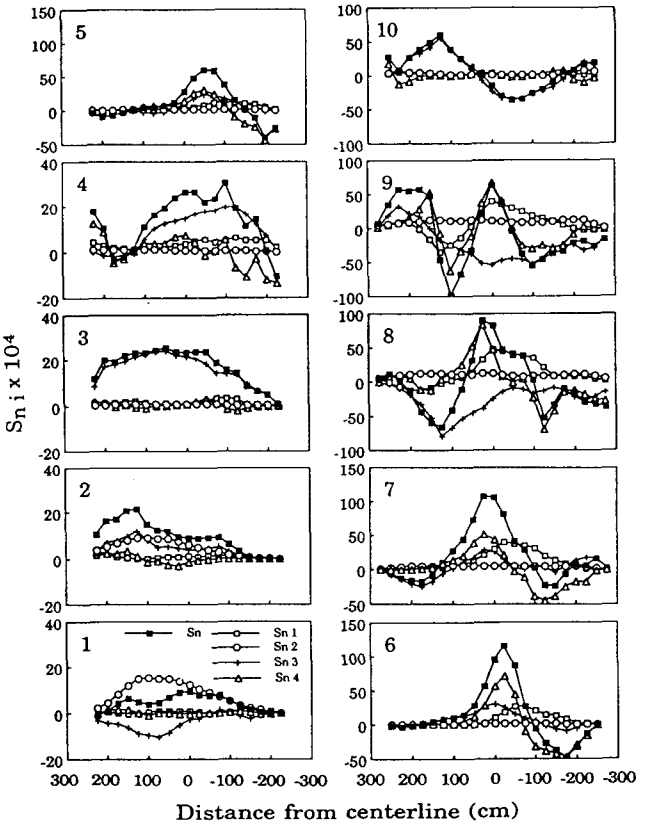

Fig. 14. Components of the cross-stream slope. Note ordinate scale change between sections 4 and 5.

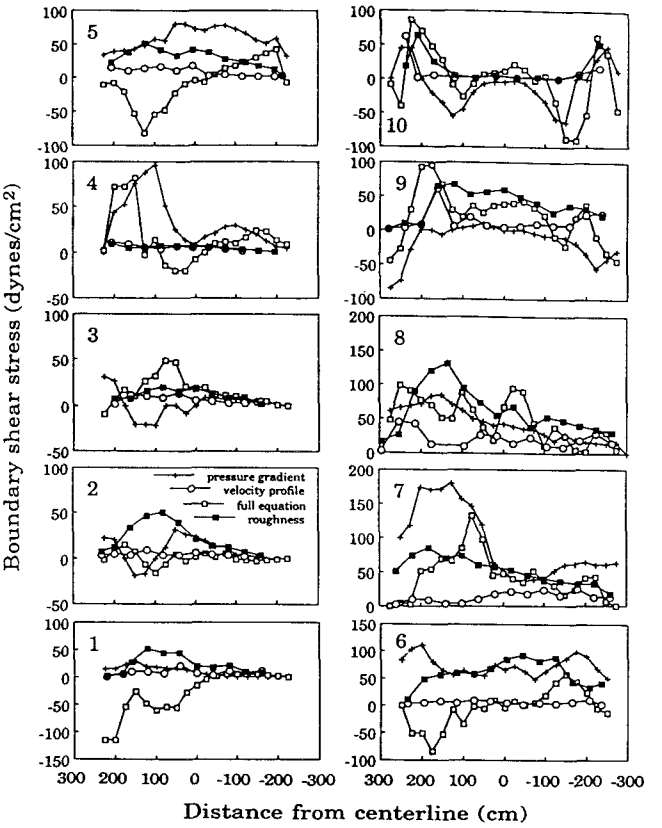

Fig. 15. Local boundary shear stress from velocity profiles, the roughness algorithm, the form-drag adjusted total boundary shear stress, and the form-drag adjusted pressure gradient force.

strong topographic change is forcing such large accelerations near the bed (Figure 8) that the profile above several centimeters gives a poor measure of the local boundary shear stress.

Another approach that to some extent circumvents the problem of the nonfully developed flow is to use an estimate of the roughness of the alluvial surface (z_0) and a single near-bed velocity measurement in the law-of-the-wall (equation (15)) to calculate the local boundary shear stress: a procedure proposed by *Dietrich* [1982] and employed successfully in a sand-bedded meander [*Dietrich and Smith*, 1984; *Dietrich and Whiting*, 1989; *Whiting and Dietrich*, 1990]. Our work in sand and gravel channels has suggested that roughness can be approximated by $z_0 = 0.1\ D_{84}$ [*Whiting and Dietrich*, 1990]. Where shoaling is strong (sections 1, 2, 5, 6, 7, and 8), the shear stress estimated from the roughness algorithm (solid squares) is substantially higher (Figure 15) than that calculated from the velocity profiles (open circles) and more reasonable. At sections 3 and 4, where depth changes are less important, the two methods give very similar results.

In order to compare the total boundary shear stress from the full equation (1) with that of the local boundary shear stress exerted on the bed, a form-drag correction must be made to account for the resistance to flow of scales larger than the skin friction. Following the general approach of *Smith and McLean* [1977], the stress associated with the roughness scales is partitioned:

$$\tau_b = \tau_{sf} + \tau_{bp} \tag{16}$$

where τ_b is the total boundary shear stress, and τ_{sf} and τ_{bp} are components associated with the skin friction and bar-pool bathymetry. An estimate of the correction can be made from the classic equation for drag over an obstacle:

$$\tau_b = \tfrac{1}{2}\rho C_{df} U_r^2 \frac{A_x}{A_b} \tag{17}$$

where C_{df} is the drag coefficient, U_r is the reference velocity, A_x is the cross-sectional area perpendicular to the flow, and A_b is the area of the bed covered by the obstacle, respectively. Assuming that the bar can be represented as a two-dimensional obstacle of height H_{bp} and length λ_{bp} ($A_x = H_{bp}B$ and $A_b = \lambda_{bp}B$) and that the logarithmic profile is a reasonable approximation of the velocity structure, the following equation can be derived following *Nelson and Smith* [1989*a*]:

$$\frac{\tau_{bp}}{\tau_{sf}} = \frac{C_{fd} H_{bp}}{2k^2 \lambda_{bp}} \left[\ln \frac{H_{bp}}{z_{0,sf}} - 1 \right]^2 \tag{18}$$

The roughness $z_{0,sf}$ was calculated with the roughness algorithm for the average D_{84} of 16.0 mm. For the observed values of H_{bp}, λ_{bp}, and z_0 of 0.80, 15, and 0.0019 m, respectively, and assuming flow to separate so the form-drag coefficient has a value of 0.21 [*Smith and McLean*, 1977], the form-drag ratio equals 1.8. Despite the approximate nature of the form-drag ratio (18), a similar ratio of 1.5 was estimated for flume channels with similar planform and topography by an independent means: the local boundary

shear stress back-calculated from sediment transport measurements was a factor of 1.5 smaller than the average pressure gradient force over a length of channel that included many bends and bars [*Whiting*, 1990].

The form-drag adjusted shear stress (open square) predicted with the full equation is only grossly similar to the local boundary shear stresses predicted from the roughness algorithm (Figure 15). The average of the two form-drag ratios, 1.65, was used. Shear stresses in both cases are small at the exit of the bend, increase over the bar, then drop to low values past the bar (Figure 15), but overall the comparison is not very encouraging. The predicted local boundary shear stress, from consideration of the force balance, is variable spatially and often systematically different from the other estimates of the stress. The difficulty, at least in part, is that the full-equation-derived shear stress is the sum of several larger terms of opposite sign. Errors in the large component terms when summed overwhelm the typically smaller stress term. For instance, incorrect measurement of the water surface elevation by 1 mm, given the typical 2-m spacing of sections, causes an average error in stress of 20 dyn/cm^2. This data set was collected with very closely spaced sections and detailed measurements of flow, indicating that boundary shear stress prediction from the divergence of the measured velocity field is very difficult. The much better prediction of the slope values is due to the pressure gradient force being one of the larger terms in the balance. It is interesting that the estimate of stresses from the form-drag adjusted pressure gradient force (crosses) gives as reasonable a picture of the local boundary shear stress as the form-drag adjusted total boundary shear stress (Figure 15).

Despite the variability of the full-equation-derived shear stress, the components can be used to examine the balance of forces as flow accelerates over and around the channel bar. The magnitude of the components of the downstream total boundary shear stress field from the right side of equation (1) are mapped in Figure 16. Pressure gradient force is small in the upstream portions and locally negative (Figure 16*a*). Downstream it increases as the water surface steepens and the flow shoals. The highest values are along the left bank where shoaling is strong. Past the bar, as flow deepens, negative values reflect the decelerating flow. The downstream transport of downstream momentum, the second term on the right side of (1) (Figure 16*b*), is negative over much of the reach, a consequence of the downstream acceleration with shoaling. Past the bar top the positive values show the deceleration in deeper flow. The negative values in Figure 16*c* in the areas adjacent to the bar top are due to the lateral flux of the downstream momentum (the third term on the right side of equation (1)) into the marginal channels. The negative values in the upstream bend reflect the cross-stream flux of the downstream momentum toward the left bank. The stress associated with the curvature is not mapped because of the small contribution it makes to the force balance in this relatively straight reach.

As discussed earlier, the roughness algorithm gives the most coherent and consistent estimate of the stress distribution through the channel reach. The spatial variation in local boundary shear stress from the roughness algorithm (Figure 17) is related to the topographic variation (Figure 1) and the spatial distribution of grain size (Figure 4). Moderate values of shear stress in the upstream bend diminish in the deeper flow. Stresses are particularly low along the right bank in the

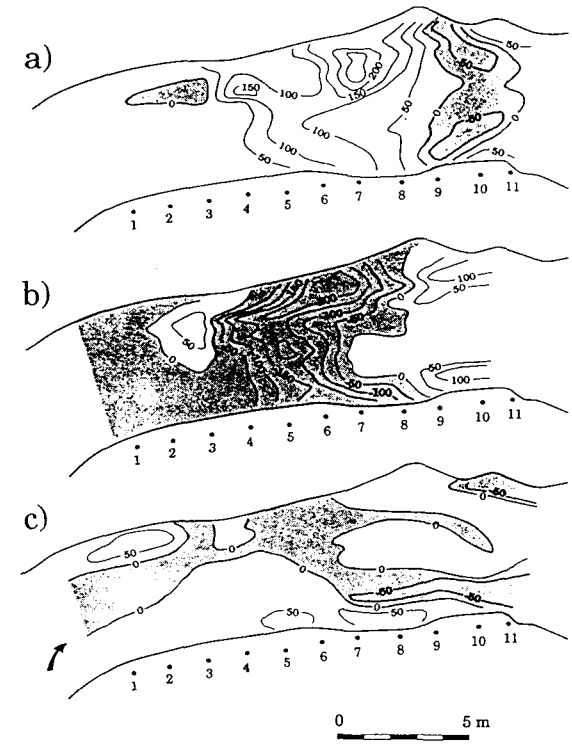

Fig. 16. Maps of components of the total downstream boundary shear stress, (*a*) Pressure gradient force, (*b*) streamwise transport of downstream momentum, and (*c*) cross-stream transport of downstream momentum.

lee of the point bar. This is consistent with the deposition of sand in this area. Shear stresses increase substantially with shoaling to values that approach the threshold for motion. The map of grain size (Figure 4) can be used to estimate the local critical boundary shear stress, hence it is a basis for placing constraints on calculated local boundary shear stress [*Dietrich and Whiting*, 1989]. For gravel, and with dimensionless critical shear stress ($\tau_{*cr} = \tau_b/[\rho_s - \rho)gD_{50}]$) equal to 0.06, multiplication of the grain diameter in millimeters by ten gives the critical boundary stress for motion in dynes/cm^2 to within 3%. The highest stresses are along the left bank near where the pressure gradient force is large and over the bar top; correctly, these values do not exceed the critical shear stress. Two corridors of higher stress project along either side of the bar. Past the bar front, shear stresses are very low.

The stress divergence shown in Figure 17 suggests that at the measured stage and higher, topographic modification would occur, were it not for the strong spatial variation in the surface

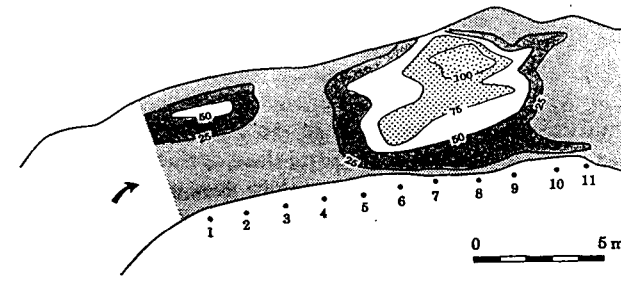

Fig. 17. Map of the local boundary shear stress from the roughness algorithm.

grain size and hence critical boundary shear stress. Solfatara Creek is a compelling example of the influence of spatial segregation upon the stable morphology of a channel bed and illustrates a fundamental difference between sand and gravel channels. In sand-bedded channels, boundary shear stress is typically many times the critical value for sediment entrainment, yielding erosion or deposition to force lateral sediment flux or bathymetric stress adjustment in response to stress divergence. In contrast, typical boundary shear stress in gravel bed channels does not greatly exceed the critical value for entrainment of the median grain size. Consequently, stress divergence can be accommodated by grain sorting without erosion or deposition [*Dietrich and Whiting*, 1989].

SUMMARY

The analysis of low flow in Solfatara Creek provides important insight into the force balance operating over alternate bar topography. Large changes in downstream velocity are associated with cross-sectional area changes and, particularly, rapid shoaling and deepening. The downstream flow field can be characterized as having a single high-velocity core in the upstream pool that bifurcates downstream around the central bar. Velocities vary in the core from near 43 cm/s in the pool to 73 cm/s over the bar margins. Maximum velocities are reached near both banks, demonstrating how channel bars can force bank erosion. The shoaling from the upstream pool to the bar crest induces strong cross-stream discharge. With initial shallowing the transverse flow is largely toward the right bank, but as the crest is approached, flow spills off the central bump toward both banks. As lateral pools deepen downstream, two well-defined secondary cells of opposing circulation develop. Weak downstream water surface slopes steepen as the bar crest is approached and then flatten. Analysis of fluid forces in the absence of significant curvature indicate that convective acceleration terms are very large in both the cross-stream and downstream directions. What distinguishes this study from the point bar case is the importance of both convective terms in the cross-stream force balance. While the magnitude of convective accelerations can be expected to diminish at higher stages relative to those studied here, theory should eventually treat the range of flows that are seen in the channel. Finally, the local boundary shear stress varies enormously over the bed. If there were not strong size sorting, we would expect modification of the topography that would fill the pools and erode the bar top. This would strongly reduce the topographic variation and diminish the relative magnitude of convective terms.

NOTATION

A_b area of bed covered by obstacle.
A_x projected area of obstacle into flow.
B transverse width of obstacle.
C_d channel drag coefficient.
C_{df} drag coefficient associated with obstacle.
D_i particle diameter such that i percent is finer.
E water surface elevation.
H height of bar.
N n/R.
Q_{nw} cross-stream flow discharge summed across the channel.
Q_{sw} downstream flow discharge.
R centerline radius of curvature.
S downstream water surface slope, $-dE/[1 - N)ds]$.
S_1, S_2, S_{3a}, S_{3b} components in force balance controlling downstream water surface slope.
S_n cross-stream water surface slope (dE/dn).
$S_{n_1}, S_{n2}, S_{n3}, S_{n4}$ components in force balance controlling cross-stream water surface slope.
g gravitational acceleration.
h local flow depth.
k von Karman's constant assumed equal to 0.40.
k_s characteristic roughness size, here equal to D_{84}.
n cross-stream coordinate.
s downstream coordinate.
u_n velocity component in the n (cross-stream) direction.
u_s velocity component in the s (downstream) direction.
w width of channel.
z near-vertical coordinate.
z_0 bottom roughness scale.
β near-bed flow direction relative to s.
λ wavelength of bar.
θ direction of flow.
ρ fluid density.
ρ_s sediment density.
τ_{*cr} dimensionless critical boundary shear stress for sediment entrainment.
τ_{pb} component of total boundary shear stress associated with bar-pool topography.
τ_{sf} component of total boundary shear stress associated with skin friction.
τ_{zn} shear stress on the z plane in the n direction.
τ_{zs} shear stress on the z plane in the s direction.
$\langle\rangle$ vertically averaged quantity.
$(\,)_b$ quantity at the boundary.
$(\,)_c$ value from continuity.
$(\,)_m$ measured quantity.

Overbars are used to indicate cross-sectionally averaged quantities.

Acknowledgments. George Ehlers assisted in the field work. We benefitted from discussions with Jon Nelson and J. Dungan Smith. D. Loewenherz, D. Montgomery, and M. Seidl and three anonymous reviewers improved the manuscript. We thank the superintendent and research staff of Yellowstone National Park for permission to work in the park and for their cooperation during the study. Computational assistance from Cathy Wilson-Rich was appreciated. Acknowledgment is made to the Donors of The Petroleum Research Fund administered by the American Chemical Society for support of this research (ACS-PRF-18427-AC2).

REFERENCES

Blondeaux, P., and G. Seminara, A unified bar-bend theory of river meanders, *J. Fluid Mech.*, *157*, 449–470, 1985.

Bluck, B. J., Sedimentation in the meandering River Endrick, *Scot. J. Geol.*, *7*(2), 94–138, 1971.

Bridge, J. S., and J. Jarvis, The dynamics of a river bend; a study in flow and sedimentary processes, *Sedimentology*, *29*, 499–541, 1982.

Dietrich, W. E., and J. D. Smith, Influence of the point bar on flow through curved channels, *Water Resour. Res.*, *19*(5), 1173–1192, 1983.

Dietrich, W. E., and J. D. Smith, Bedload transport in a river meander, *Water Resour. Res.*, *20*(10), 1355–1380, 1984.

Dietrich, W. E., and P. J. Whiting, Boundary shear stress and sediment transport in river meanders of sand and gravel, in *River Meandering*, *Water Resour. Monogr. Ser.*, vol. 12, edited by S. Ikeda and G. Parker, pp. 1–50, AGU, Washington, D.C., 1989.

Engelund, F., Flow and bed topography in channel bends, *J. Hydraul. Div. Am. Soc. Civ. Eng.*, *100*(HY11), 1631–1648, 1974.

Friedkin, J. F., A laboratory study of the meandering of alluvial rivers, report, 40 pp., U.S. Waterways Exp. Stn., Vicksburg, Miss., 1945.

Helley, E. J., and W. Smith, Development and calibration of a pressure-difference bedload sampler, *U.S. Geol. Surv. Open File Rep. 73–103*, 1971.

Hooke, J. M., and A. M. Harvey, Meander changes in relation to bend morphology and secondary flows, in *Modern and Ancient Fluvial Systems*, *Spec. Publ. 6*, edited by Collinson, J. D. and J. Lewin, pp. 121–132, International Association of Sedimentology, Liege, Belgium, 1983.

Hooke, R. L., Distribution of sediment transport and shear stress in a meander bend, *J. Geol.*, *83*, 543–565, 1975.

Ikeda, H., Sedimentary controls on channel migration and origin of point bars in sand-bedded meandering rivers, in *River Meandering*, *Water Resour. Monogr. Ser.*, vol. 12, edited by S. Ikeda and G. parker, pp. 51–68, AGU, Washington, D.C., 1989.

Ikeda, S., Prediction of alternate bar wavelength and height, *J. Hydraul. Div. Am. Soc. Civ. Eng.*, *110*(4), 371–386, 1984.

Ikeda, S., G. Parker, and K. Sawai, Bend theory of river meanders, 1, Linear development, *J. Fluid Mech.*, *112*, 363–377, 1981.

Keller, E. A., and W. N. Melhorn, Bedforms and fluvial process in alluvial stream channels; selected observations, in *Fluvial Geomorphology*, *Publ. Geomorphol.*, edited by M. Morisawa, pp. 260–268, State University of New York, Binghamton, 1973.

Kinoshita, R., An investigation of channel deformation of the Ishikari River (in Japanese), *Publ. 36*, Nat. Resour. Div., Minist. of Sci. and Technol., Tokyo, Japan, 1961.

Leopold, L. B., Water surface topography in river channels and implications for meander development, in *Gravel-bed Rivers*, edited by R. D. Hey, J. C. Bathurst, and C. R. Thorne, pp. 359–388, John Wiley, New York, 1982.

Leopold, L. B., and M. G. Wolman, River meanders, *Geol. Soc. Am. Bull.*, *71*, 769–794, 1960.

Nelson, J., and J. D. Smith, Flow in meandering channels with natural topography, in *River Meandering*, *Water Resour. Monogr. Ser.*, vol. 12, edited by S. Ikeda and G. Parker, pp. 69–102, AGU, Washington, D. C., 1989.

Odgaard, A. J., Meander flow model, I, Development, *J. Hydraul. Div.*, *112*(3), 1117–1136, 1986.

Odgaard, A. J., and M. A. Bergs, Flow processes in a curved alluvial channel, *Water Resour. Res.*, *24*(1), 45–56, 1988.

Parker, G., On the cause and characteristic scales of meandering and braiding in rivers, *J. Fluid Mech.*, *76*(3), 457–480, 1976.

Richmond, G. M., and H. A. Waldrop, Surficial geologic map of the Norris Junction Quadrangle, Yellowstone National Park, Wyoming, U. S. Geol. Surv., Reston, Va., 1975.

Seminara, G., and M. Tubino, Alternate bars and meandering, in *River Meandering*, *Water Resour. Monogr. Ser.*, vol. 12, edited by S. Ikeda and G. Parker, pp. 267–320, AGU, Washington, D. C., 1989.

Smith, J. D., Measurement of turbulence in ocean boundary layers, paper presented at Working Conference on Current Measurement, Office of Ocean Eng., Natl. Oceanic and Atmos. Admin., Univ. of Del., Newark, Del., Jan. 11–13, 1978.

Smith, J. D., and S. R. McLean, Spatially averaged flow over a wavy surface, *J. Geophys. Res.*, *83*, 1735–1746, 1977.

Smith, J. D., and S. R. McLean, A model for meandering rivers, *Water Resour. Res.*, *20*(9), 1301–1315, 1984.

Thorne, C. R., L. W. Zevenbergen, J. C. Pitlick, S. Rais, J. B. Bradley, and P. Y. Julien, Direct measurements of secondary currents in a meandering sand-bed river, *Nature*, *316*, 746–747, 1985.

Whiting, P. J., Bar development and channel morphology, Ph.D. diss., 203 pp., Univ. of Calif., Berkeley, 1990.

Whiting, P. J., and W. E. Dietrich, Boundary shear stress and roughness of mobile alluvial beds, *J. Hydraul. Eng.*, *116*, 1495–1511, 1990.

Yen, C. L., and B. C. Yen, Water surface configuration in channel bends, *J. Hydraul. Div. Am. Soc. Civ. Eng.*, *97*(2), 303–321, 1971.

W. E. Dietrich and P. J. Whiting, Department of Geology and Geophysics, University of California, Berkeley, CA 94720.

(Received December 11, 1989;
revised August 17, 1990;
accepted January 4, 1991.)